Available online at www.sciencedirect.com
ScienceDirect
Engineering Geology 100 (2008) 101 – 119
ENGINEERING GEOLOGY
www.elsevier.com/locate/enggeo

Neotectonics and slope stabilization at the Alhambra, Granada, Spain

J.L. Justo [a,*], J.M. Azañón [b,c], A. Azor [b], J. Saura [d], P. Durand [a], M. Villalobos [e], A. Morales [a], E. Justo [a]

[a] Department of Continuum Mechanics, E.T.S. Arquitectura, University of Seville, Seville, Spain
[b] Department of Geodynamics, University of Granada, Campus Fuentenueva s/n, Granada 18002, Spain
[c] Instituto Andaluz de Ciencias de la Tierra, University of Granada—C.S.I.C., Campus Fuentenueva s/n. Granada 18002, Spain
[d] Confederación Hidrográfica del Guadalquivir, Seville, Spain
[e] Tecna, Granada, Spain

Received 18 June 2007; received in revised form 11 December 2007; accepted 15 December 2007
Available online 15 January 2008

Abstract

Over 600 years, the Alhambra Palace of Granada, Spain, (a World Heritage site) has been damaged by earthquakes and slope instability. The western part of San Pedro Cliff, on the northern slope of the palace is a compound fault scarp — fault-line scarp, modified by river erosion and latterly by successive slab falls. The plane of the fault with the largest throw (c. 7 m) outcrops in the innermost part of the escarpment, and is a normal fault with a NW–SE strike and steep SE dip. It is part of a set outcropping along the Alhambra hill. Fault activity may be very recent, perhaps related to historical earthquakes. Seismic risk at the Alhambra is considered to be moderate: there is earthquake damage of the Arab walls and barrier. The most significant historical damage occurred in 1431 and partially collapsed the Arab barrier. Extension associated with the faults loosens the ground and contributes to slab falls. The faults are also preferential water paths. Both the many cracks of the walls and collapses of the Alhambra barrier appear concentrated and aligned with the fault set.

Stability analyses suggest that the factor of safety of the San Pedro slope under 1000-yr-return-period earthquake loading may drop below 1.0 and the critical slip surface could penetrate the Alhambra walls. To raise the safety factor above 1.0 and to counteract extensional stress in the cliff, an apparently environmentally acceptable solution with minimal visual impact is proposed. It consists of high-yield-stress wire mesh, post-tensioned by anchors, and coloured to blend with the cliff.

Keywords: Tectonics; Normal faults; Alhambra; Stability of slopes; Environmental impact; Wire mesh; World Heritage preservation

1. Introduction

The Alhambra (Fig. 1) is one of the most important national monuments in Spain, visited annually by up to 2 million domestic and international tourists. This monument, a World Heritage site, is located on the top of a red hill that dominates a plain, the Granada basin, where most of Granada city is located. One of the most incised rivers of the region, the Darro, which drains into the depression, is situated in the eastern part of the town. The Alhambra's walls are close to escarpments generated by incision of this river. Slope stability of the escarpments on this side of the Alhambra hill has been a critical problem since the construction of this palace. In this area, the 65.5 m high San Pedro Cliff (Fig. 1), a dihedral 65.5 m high, is the steepest escarpment of the Alhambra hill. This eroding cliff reaches to 23.8 m from the Alhambra palace wall. Retreat of this cliff has occurred through superficial slab falls mainly induced by the floods of the Darro River, the loosening produced by the extensional tectonic regime, erosion, seepage coming from Alhambra palace and earthquakes. Fig. 2 shows, at the top, the southern part of the Iberian Peninsula and the Granada basin in an inset. This depression (Fig. 2, centre) is located in the central sector of the Betic Cordillera, and is one of the most seismically active zones in the Iberian Peninsula (e.g., Morales et al., 1999; Muñoz et al., 2002; Sanz de Galdeano et al., 2003; Galindo-Zaldívar et al., 2003). In this respect, the most important

* Corresponding author. E.T.S. Arquitectura—Avenida Reina Mercedes, 2-41012 Sevilla, Spain. Tel.: +34 954556588; fax: +34 954556965.
E-mail address: jlj@us.es (J.L. Justo).

0013-7952/$ - see front matter © 2008 Elsevier B.V. All rights reserved.
doi:10.1016/j.enggeo.2007.12.007

Fig. 1. South view of San Pedro Cliff, showing to the right the fault-line scarp. Above stand the Alhambra walls and, at the foot, River Darro and Albaicín houses.

earthquake affecting the Alhambra and neighbouring areas occurred in 1431, and was responsible for the partial collapse of the Arab barrier (Azañón et al., 2004). The Christian wall, built in 1526, has also been partially destroyed (Figs. 1 and 11) by rockfalls related to tectonic activity.

In this paper, an analysis is made of the roles of active faults, tectonic discontinuities and cracks on the slope stability of the northern side of the Alhambra hill. The structural, stratigraphic and geomorphologic characteristics of San Pedro cliff are described in order to consider the conditioning and triggering factors of mass movements causing retreat of this cliff. Finally, a solution is proposed to stabilize the main escarpments of San Pedro cliff with minimum visual impact. This solution considers the high seismic hazard of this region.

2. Geological setting

The Alhambra palace was constructed on the top of a hill, on a conglomeratic sequence that constitutes the Alhambra formation. The city of Granada is located at the base of the Alhambra hill, on a plain, surrounded by mountains. From a geological point of view, this plain is known as the Granada basin (Fig. 2), which underwent continuous subsidence between the Upper Miocene and the Quaternary, under marine conditions between 6/7 and 11 Ma ago and with continental infilling until approximately 0.5 Ma ago. The sedimentary cover is up to 1.5 km thick (Rodríguez-Fernández and Sanz de Galdeano, 2006). The oldest sediments are conglomerates, calcarenites and marls deposited in marine environments during a lower Tortonian age (9–10 Ma). Marine sedimentation continued until the uppermost Tortonian period (>7.5 Ma) (Rodríguez-Fernández et al., 1989). Uplift during the Messinian age (6–7 Ma) isolated the basin from other surrounding ones (e.g. Alboran Sea), which later evolved into continental environments with a similar paleogeography. The continental sediments are conglomerates, siltstones, sandstones and limestones, deposited in the central parts of the basin in lakes or by rivers that drained the surrounding mountains.

The Alhambra conglomerates correspond to alluvial fans, upper Pliocene–lower Pleistocene in age, known as the Alhambra formation, mostly constituted of rounded stones with an average size of 10 cm. The matrix (<0.08 mm) ranges between 13 and 35% and is generally sandy silt, sometimes clayey. There are also 1 m thick layers, of clayey silt. Alluvial fans have been made from erosion of the basement of the Granada basin outcropping in the Sierra Nevada relief. This basement is formed by metamorphic rocks (schist, phyllite and marble) of the Palaeozoic to Mesozoic protholite ages and by sediments from the Triassic to Cretaceous ages.

3. Structures, tectonic evolution and seismicity

Sedimentation in the Granada basin was controlled by several sets of faults, most notably those of E–W and NW–SE orientations (Fig. 2). Many of these faults are identified by surface mapping and seismic reflection profiles (Rodríguez-Fernández and Sanz de Galdeano, 2006). Conspicuous NW–SE faults are present in the

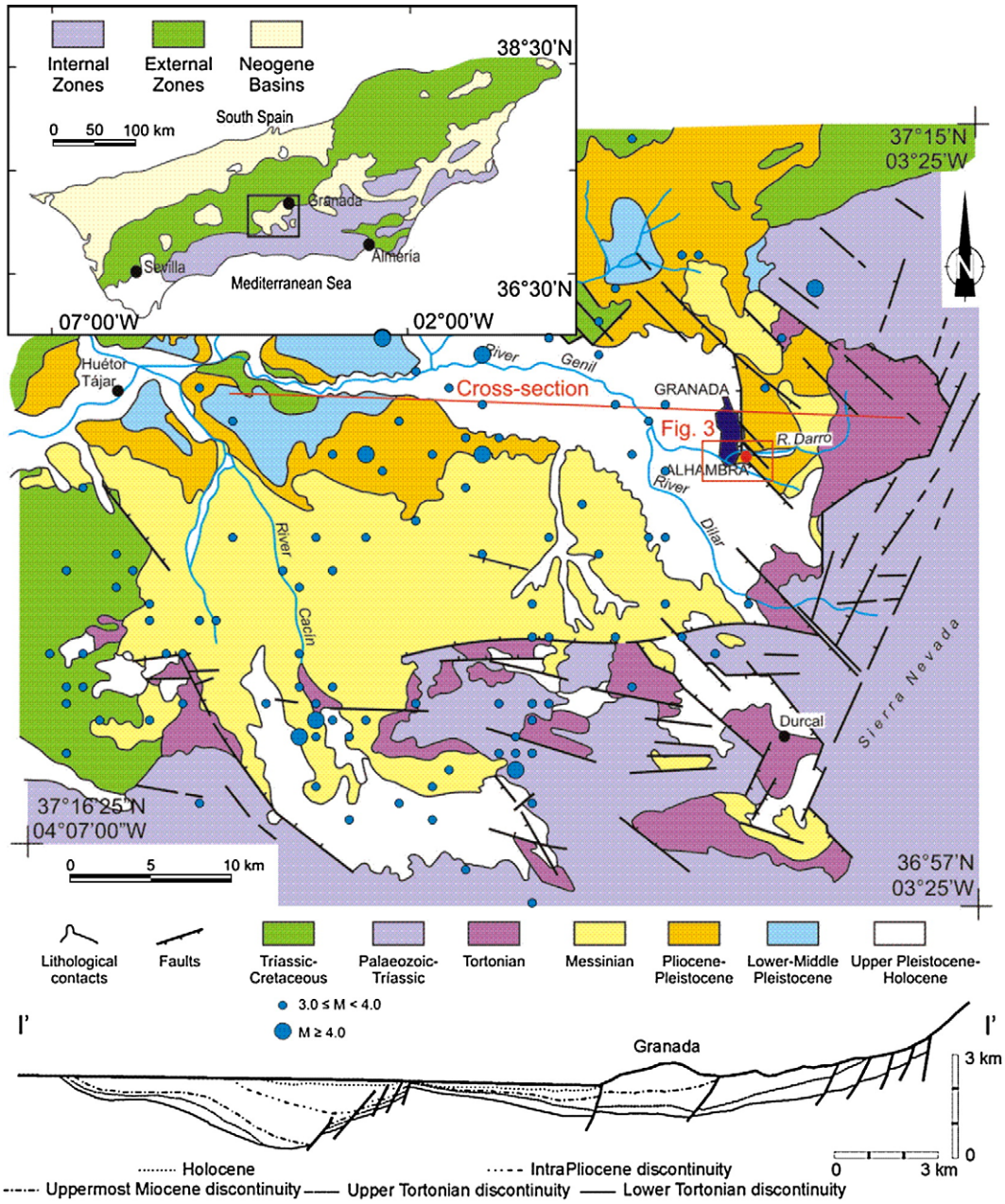

Fig. 2. In the upper part, geological map of southern Spain, prepared by the authors, showing in an inset the Granada depression. At the centre, geological map of Granada basin, with inset of the site. At bottom cross-section. Epicentres with $M_{bLg} \geq 3$ registered during the period 1978–2007.

eastern part of the basin (Fig. 3), some of which limit the Granada basin, which have influenced the basin's stratigraphic architecture. The location of Fig. 3 is shown in Fig. 2. These faults are normal, mostly with a NW–SE orientation, and dipping towards the SW. These NW–SE faults cross-cut and displace previous E–W faults, defining the main subsiding areas of the central and eastern part of the basin. The Bouguer gravity map of the Granada basin shows that within the basin there are several more sectors that are subsident, where significant negative gravity values occur (Rodríguez-Fernández and Sanz de Galdeano, 2006).

These faults produce large steps in the relief (Fig. 4). In this way, the boundary between the basement and sedimentary cover always coincides with normal faults that dip towards the basin. The faults are characterized by large fault scarps with associated slickensides and striations, with dimensions ranging from metres to decametres (e.g. the Nigüelas fault); the footwalls of these faults are uplifted, and show strong relief with deeply incised drainage. Several steps are found between the flat area of the Granada basin and the ranges where the basement outcrops, which could represent fault scarps, variably degraded by erosion of the soft sediments. The strike of these steps is NW–SE (Fig. 3), in accordance with the strike of the majority of the normal faults mapped on the margin of the basin. The topographical step between Llano de la Perdiz and the Alhambra hill is probably related to one of these faults, showing continuity with the step located between the Cerro de San Miguel and Albaicín quarters.

Fig. 3. Relationship between the following steps in the relief and faults: Llano de la Perdiz–Generalife, San Miguel hill–Albaicín, Generalife–Alhambra and Alhambra–Granada.

Basin ward migration of the extensional front has exhumed the footwalls of older faults, uplifting the previous Tortonian sedimentary cover, which presently outcrops in emerged ranges on the margins of the basin. This process has also affected the Pliocene and Quaternary sediments that presently constitute the hanging-wall blocks in the eastern and northeastern boundaries of the Basin, foothills where most of Granada city is located. The sedimentary formations show unconformable relationships in the margins of the basin which correlate with paraconformities towards the centre of the basin; however, in many places the present boundaries are normal faults.

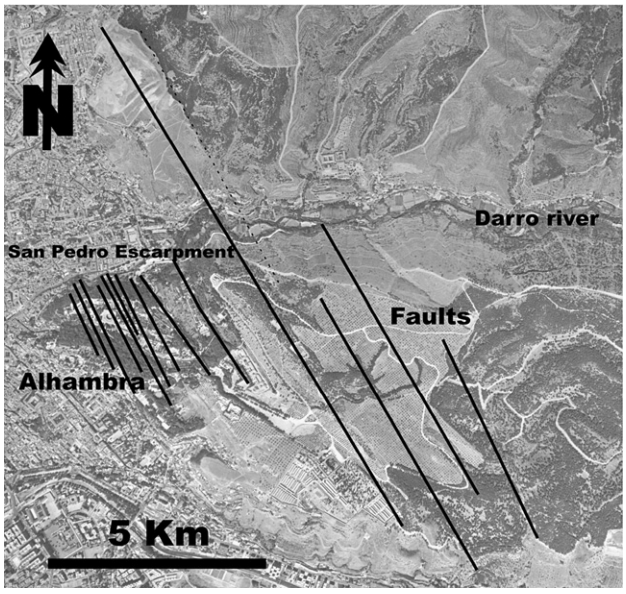

Fig. 4. NW–SE normal faults in the surroundings of San Pedro Cliff.

The Iberian Peninsula has been divided into 27 seismogenic areas (Martín, 1984), with assumed homogeneous seismic and tectonic characteristics. The year of completeness of the seismic catalogue for the Granada basin (1978) is the starting point for the studies performed based upon earthquake sources. All studies have been carried out for magnitudes $M_{bLg} \geq 3$. Parameters of the Gutenberg–Richter relationship were obtained using the maximum likelihood method. The least-squares method fits to the Gutenber–Richter formula, but tends to statistically estimate too low a b value, because it cannot include magnitudes above the maximum observed (Bender, 1984). Utsu (1965) proposed a different estimated b value, which was shown by Aki (1965) to be a maximum likelihood estimate for the particular exponential model, which can be derived from the log Gutenberg–Richter relationship. Maximum likelihood formulas give biased results if they are applied to interval data, with bias increasing as interval size increases. The bias is small at magnitude intervals $\Delta M = 0.1$, as is the case in this study. The b-value estimate has been obtained according to the formulas given by the authors cited above and others

(Page, 1968; Lombardi, 2003) which are widely used in earthquake engineering. The Granada basin, with a surface of 3835 km^2, has the maximum annual rate of earthquakes per unit surface in the Iberian Peninsula: 1.34×10^{-3} events per km^2. Fig. 2 shows the epicentres of magnitude ≥3. The Gutenberg–Richter relationship (Fig. 5) is:

$$\log N\left(M_{bLg}\right)\geq 5.76 - 1.41M_{bLg} \quad (1)$$

where $N(M_{bLg})$ is the annual rate of earthquakes with a magnitude ≥ M_{bLg}.

The reason for using a log representation is to obtain a linear relationship.

Fig. 6A shows the cumulative probability magnitude–density distribution of earthquakes. Seismic activity in the Granada basin is high, with many earthquakes, all of them of moderate to low magnitude ($M_{bLg}\leq 6.0$). There have been important historical earthquakes, which produced great material damage (Tercedor, 1951); however, it is difficult to evaluate their magnitude. Fig. 6B shows the cumulative probability focal-depth density distribution: more than 70% of all the events have a focal depth of ≤10 km. The focal mechanisms of recent earthquakes indicate a stress field dominated by a tension tensor with an associated NE–SW extensional axis. The extension coincides with paleo-stress determinations from Tortonian and earlier sediments, and is compatible with NW–SE striking normal faults with the same associated extensional transport (Galindo-Zaldívar et al., 1999). Within proximity of the Alhambra Palace, active normal faults are responsible for the topographic steps.

4. Cracks and faults in the Alhambra hill: origin and evolution of San Pedro escarpment

The present relief of the margins of the Granada basin is strongly determined by the throw of the normal faults, and also by river erosion (Genil, Darro, Monachil, etc.). The drainage system of the Granada basin is a tributary to the Guadalquivir River since its capture during the upper Pleistocene era. The Alhambra hill is a local divide between two important rivers draining from the Sierra Nevada to the Granada depression: the Darro and Genil Rivers. The present configuration of these two rivers evolved over the last 0.5 Ma. The drainage pattern of the Darro River was incised in the conglomerates of the Alhambra Formation. San Pedro escarpment is a 65.5 m high cliff, situated at a meander of the Darro River, which has progressed to a distance of 23.8 m from the Alhambra palace wall. This escarpment has been produced by superficial slab falls, initially induced by erosion at the external part of the meander during flooding of the Darro River (Fig. 7), but now mainly due to loosening produced by the extensional tectonic regime, superficial erosion, seepage coming from Alhambra palace and earthquakes. Floods of 20-yr return period have a peak discharge of 90 m^3/s (Ayala-Carcedo et al., 1986). The normal flow discharge is 0.4 m^3/s (Castillo, 2007).

Many normal faults with a N130–N150 strike, dipping 65–75° both towards the SW (mostly) and the NE (subordinate) are exposed in the northern slope of the Alhambra hill (Fig. 7); wherever it has been possible to observe them, they present only a dip slip, with no strike slip. The displacements of these faults

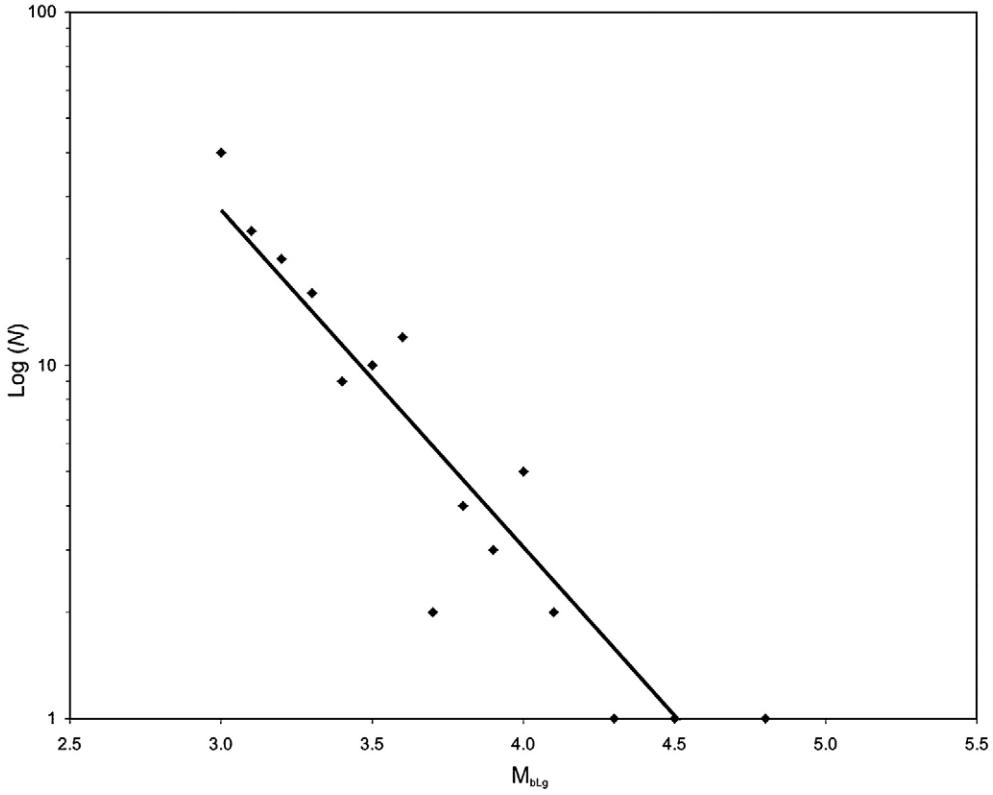

Fig. 5. Gutenberg–Richter relationship for earthquakes ≥M_{bLg}3 (1978–2007) in the Granada basin.

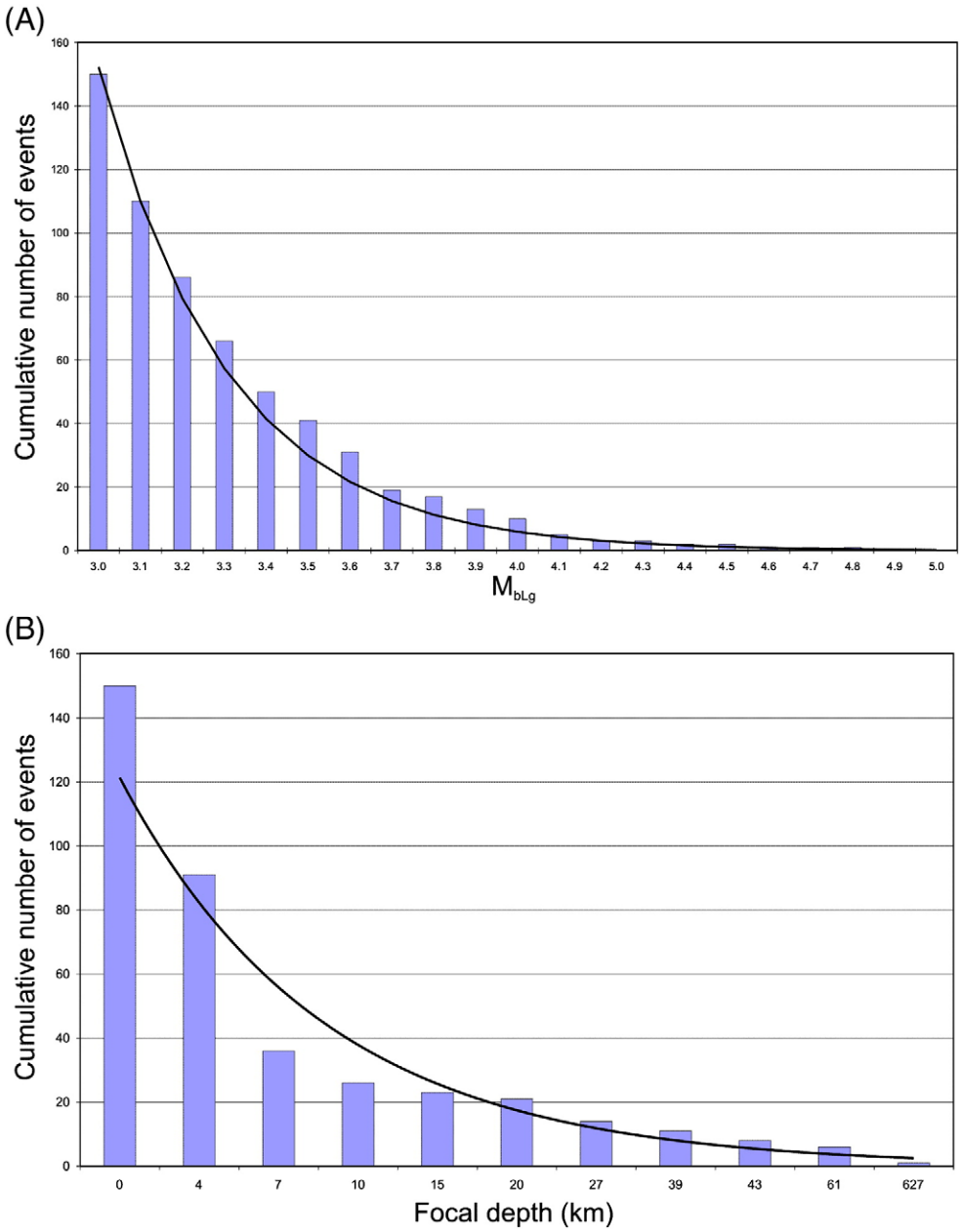

Fig. 6. Cumulative probability distribution for earthquakes $\geq M_{bLg}3$ (1978–2007) in the Granada basin. Data from IGN (Spain). A) Magnitude–frequency distribution. B) Focal-depth frequency distribution.

range between a few centimetres and 7 m. This last figure is the totalled observable throw of all faults in the area. One of the most significant faults is parallel to the western side of San Pedro escarpment dihedral (with N 150° E strike) and has a minimum throw of 7 m (Fig. 8). This side of the cliff corresponds to a fault-line scarp, as the cliff orientation here is controlled by the fault. It is an erosional cliff, as it has suffered some retreat due to successive superficial slab falls and other erosion processes active on the cliff. As may be observed in the scar in Fig. 1, the most recent slab fall occurred on this cliff face (in 1985) and affected up to 30% of its extension. Notwithstanding the spectacular nature of the accident, the fall volume was not too large, because the slab thickness was relatively thin. This set of faults developed a fault rock with pebble clasts reoriented to be parallel to the dip of the fault (Fig. 9). The matrix of the conglomerate is also disturbed with many shear surfaces parallel to the fault walls. Slickensides are common, always indicating shear displacement in the direction of the dip slip. Fractured clasts are found within and near the faults. The joints are parallel to the faults' strike and are compatible with tension gashes produced in the same stress field that generated the faults.

A precise levelling of the cliff has given an average dip angle, α, of 70° for the fault. The cliff is erosional so its slope does not directly show the fault dip. However, this may be approximately true, because the slide surface is nearly parallel to the slope in the slab fall that occurred in 1985 and in some incipient falls that may be presently seen. The extensional tectonic regime reduces the horizontal stresses up to failure

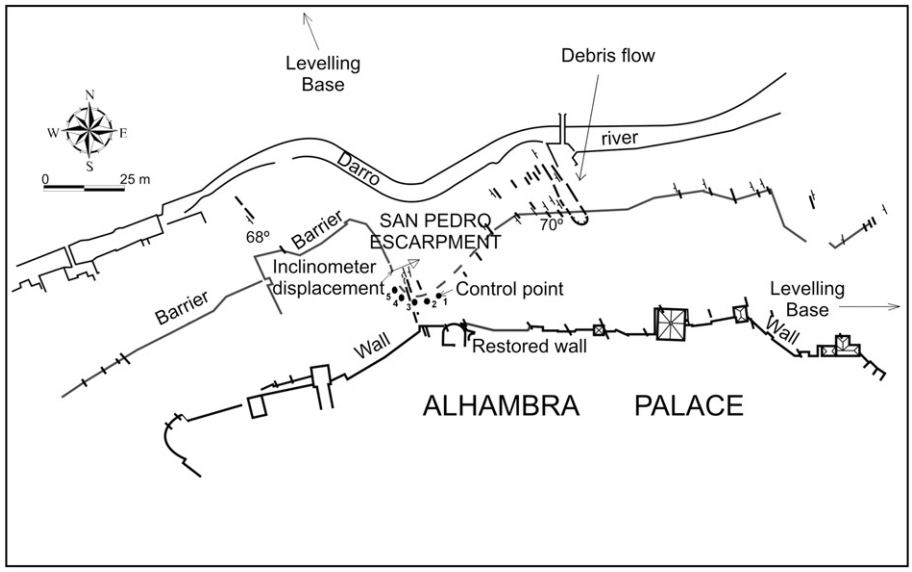

Fig. 7. Outline of the site showing the river meander, the main cracks at *La Alhambra* and Christian wall, faults at the hill slope, the position of the landmarks and levelling bases and the direction of the resultant vector of the inclinometer displacements.

along the normal fault. Supposing that, for shear failure, the fault plane coincides with the plane of contact of the Mohr circle with the strength envelope (v. Ferrill and Morris, 2003), the relationship between the dip angle and the angle of internal friction is:

$$\phi' = 2\alpha - 90° = 50°. \quad (2)$$

Consequently, these fractures are considered syngenetic with the faults. Some of the clasts are fractured and displaced by the faults, with textures that we relate with the co-seismic activity of these faults. Displacement along these faults implies release of seismic energy during short periods of time (nearly instantaneous) followed by long aseismic periods of quiescence. Locally, the bedding in the conglomerates is tilted in the hanging-wall of the faults, always towards the footwall. Drag folds were observed in some of the faults, indicating normal displacement.

The activity of these faults is more recent than the Lower Pleistocene age estimated for the Alhambra Formation. Quaternary and recent activity of these faults is reasonable considering that they are not capped by any other sediment. Between 1989 and 1993, measurements were taken from two levelling bases, 150 m away from five topographic landmarks

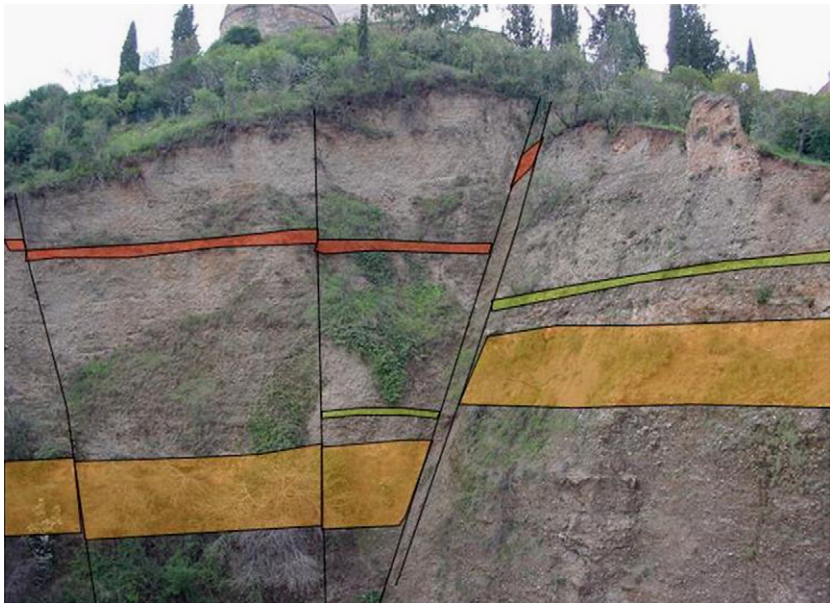

Fig. 8. View of the dihedral, showing the fault throw. Red level is a palaeosol ascribed to Pleistocene. Green colour outlines a silty stratigraphic level on both sides of fault. Yellow level is a quartzite sandstone bed which can be recognised in the footwall and hanging-wall of the fault.

Fig. 9. Rotated pebbles, orientated parallel to the fault plane by shear strain in Alhambra conglomerate.

placed on top of the escarpment (Cedex, 1993; Martínez, 1998) and located in Fig. 7. The error in these measurements is ≤5 mm. Owing to this, the measured vertical displacements are not reliable. Table 1 shows the measured horizontal displacements that indicate motion towards the river (average value 10 mm). The topographic equipment used was a Wild 72 and a Geodimeter total station. The displacements are too high to be tectonic, and perhaps could be ascribed to creep extension due to the unloading produced by the successive slab falls or weathering of conglomerate. Unfortunately the Granada basin is not determined by recent GPS surveying. Independent horizontal displacement measurements, with an error ≤1 mm, were taken in an inclinometer placed near the landmarks, but unfortunately during a very short period of time (February to October, 1994). The horizontal displacement at surface, in the direction N16°E was 3.8 mm and in the direction N106°E 4 mm. The resultant vector, in direction N60°E and nearly perpendicular to the fault, has a magnitude of 5.5 mm (Fig. 7). Recently, new inclinometers have been installed and the measurements are being taken. In any case, there is compelling evidence from observable damage that slope adjustments of some origin are a hazard to the cliff and nearby structures. The historical evidence is quite sufficient to show that there is also seismic hazard. Both hazards need to be considered in planning to conserve this World Heritage site.

Table 1
Horizontal displacement towards the river in topographic landmarks

Landmark	Horizontal displacement (mm)
1	17±5
2	8±5
3	14±5
4	5±5
5	7±5
Average	10±1

The faults would have accumulated important displacements related with associated periodic seismic activity. The most important faults of this system, apart from the fault in San Pedro cliff, would coincide with the topographical steps observed on this margin of the Granada basin (Fig. 3). The tectonic origin of these topographical steps would indicate recent fault activity, overstepping the erosional processes that tend to eliminate the tectonic relief. Furthermore, some of these faults could be active and connected to the present seismicity detected in this region.

The Alhambra and its quarter is a strategic place to detect the possible co-seismic activity of the faults that have affected the Alhambra formation during the last seven centuries. With this in mind, we mapped the more important cracks (Fig. 7) in the Alhambra walls of the northern side of the monument and those in the Christian wall. The present Christian wall was built (bordering San Pedro Cliff) ca. 1560, because the previous Arab barrier was destroyed through various causes, some of which may have been earthquakes. The chronicle of Alvar García de Santa María describes the events in chapter XXI: *at this time the earth trembled in the Real and even more in the City of Granada and a great deal more in the Alhambra* (subject to strong topographic amplification) *where it collapsed some sections of its Arab wall* (Galbis, 1932).

The most interesting features have been detected in the Christian barrier where it is cracked or collapsed. In many places, ruptures in the Christian wall show a geometrical continuity with fault planes that outcrop in the conglomerates underlying it. In some cases, fractures in the Christian wall show the same orientation as the underlying faults. In others, the barrier has been rebuilt, however the original rupture surface can be appreciated and this coincides with the strike and dip of the faults.

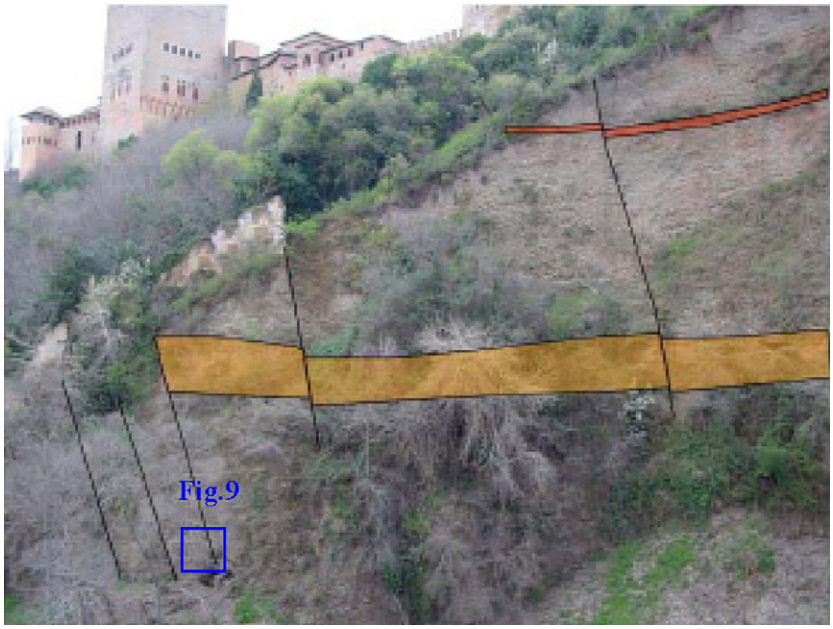

Fig. 10. Sub-parallel normal faults in San Pedro Cliff. The location of Fig. 9 is shown in an inset.

Opened cracks have also been observed in the wall, with relative displacements that are coherent with those observed in the underlying faults. If the cracks in the Christian wall and the Alhambra wall are aligned, the resultant strike is (N140°E), coinciding also with the average position of the faults that outcrop in the northern slope of the Alhambra hill. As indicated above, the resultant vector from the inclinometer measurements has a direction N60°E, nearly perpendicular to this strike.

Hence it is suggested that the faults outcropping in the Alhambra quarter have possibly had recent activity (during the 15th century and later) being responsible for observed cracks in the monument. The relative displacements observed in the Christian wall and walls are normally of several millimetres and more exceptionally of several centimetres. It is possible that these displacements might be related to the activity of some earthquake or a series of earthquakes, which include higher intensity ones, because the faults either were generated during the earthquakes or were previous features displaced in relation with seismic activity. As stated above, the measured horizontal movement indicates that there is motion in the area that is too large to be tectonic. At present, there are not enough data to know the correct answer. It is probable that the faults observed in the Alhambra quarter have accumulated many displacements related to repeated seismicity in the area after being formed. Twenty-three earthquakes with hypocentres in the Granada basin and epicentre intensity above VI are mentioned in the catalogue of the *Instituto Geográfico Nacional*, occurring since 1431. In five out of the 23, the intensity in the city of Granada was ≥ VI: the earthquakes of 1431, 1526, 1778 and 1956 (intensity VII) and 1822 (intensities VI–VII). Historical evolution of the Christian wall near the San Pedro Cliff shows that a large part of it collapsed between 1775 and 1804. This barrier has nearly disappeared on the western side of the dihedral angle of the San Pedro Cliff, coinciding with the most important fault found within the Alhambra; on the eastern side, the upper half of the Christian wall has collapsed (Fig. 1). The eastern boundary of the collapsed barrier coincides with a normal fault that sinks the western block (Fig. 10). This fault produced a rupture in the barrier. Later escarpment retreat produced the collapse of the Christian wall on its right-hand side.

Fig. 11. Crack on the Alhambra wall above a fault.

Fig. 12. Crack in Torre de la Vela.

Fig. 13. San Pedro Cliff, showing location of electrical profile perpendicular to the inferred fault F1. Santa Ana irrigation structure appears at the Cliff base. Note boreholes S-1 and S-2.

The Christian wall was built with brick and mortar. Consequently, should the origin of the Christian barrier's collapse be related with co-seismic activity of the faults, as proposed here, there must have been a coeval earthquake with an intensity that would justify such damage. The seismic series during the 13th and 14th of November of 1778, with an attributed intensity of VII (López-Casado et al., 2001), could have been responsible for the collapse of the eastern section of the Christian wall near San Pedro Cliff. Fig. 11 shows a crack in the Alhambra wall above a fault.

However, this is not the only possible explanation of the millimetre displacements associated with pre-existing fault planes. These constitute weak mechanical discontinuities that can concentrate small displacements during earthquakes with a certain magnitude produced by faults of the same system (Torcal et al., 1999). In an area with high seismicity like the Granada basin, there are many faults with the same orientation and regime that could have provoked important earthquakes in the last five centuries. We can mention the earthquakes of 1884, 1911, 1954, 1956 and 1984, the last one with its epicentre located at 40 km from the most destructive of them (the 1884 earthquake in Arenas del Rey). The 1984 earthquake was registered by different seismographs, which makes the calculation of its focal mechanism possible (Morales et al., 1996). The focal mechanism of an earthquake helps to obtain the strike and regime of the source fault. The 1984 earthquake was generated by a fault with the same orientation and regime as those described in the Alhambra quarter.

Furthermore, faults, like any other mechanical discontinuity, can play an important role as preferential conduits for fluid circulation. This can favour erosion by washing the finer matrix portion of the conglomerates in the fault zone, producing differential erosion and concentration of surface water discharge. In the Alhambra forest, several small gullies coincide with the trace of faults, and could be of this origin. Although the Christian wall could have been fractured during the earthquakes, the previously mentioned differential erosion could have contributed to further damage by eroding the rocks, which support it. The debris-flow gully found in front of Chirimias Bridge (Fig. 7) is bounded by two faults. These faults conditioned the development of this surface slope process by concentrating water circulation through them. However, it must be said that there are no important springs in this area, because of the aquifers.

The movement and tilt of the towers on the northern hill slope were controlled from January 1989 until October 1994. In the tower closer to the cliff (Torre de la Vela) there was cyclic vertical motion, with resultant settlement of less than 1 mm (v. Martínez, 1998). Fig. 12 shows a crack in *Torre de la Vela,* perhaps produced by motion towards the cliff.

5. Geotechnical properties

5.1. Site investigation

Ten boreholes were drilled in the upper, medium and lower part of the cliff, up to a depth of 45 m. In two of the boreholes drilled at the top of the escarpment, S1 and S2 (Fig. 13), pressuremeter, down-hole and cross-hole, penetration, permeability, and laboratory tests were carried out (Justo et al., 2005). The difference between the different conglomerate layers is related to maximum particle size, core recovery and stiffness as measured in pressuremeter and geophysical tests. There are no clear differences in colour.

The following layers appear from top to bottom in the geological profile:

1. Dense conglomerate, with 100 mm maximum particle size and core recovery 100%, of brown to pale gray silty matrix.
2. Very dense conglomerate, with maximum particle size of 5–8 cm and core recovery of 100%, of brown to reddish silty to clayey matrix.
3. Moderately dense conglomerate, with core recovery of 60%, of brown to pale gray silty matrix.

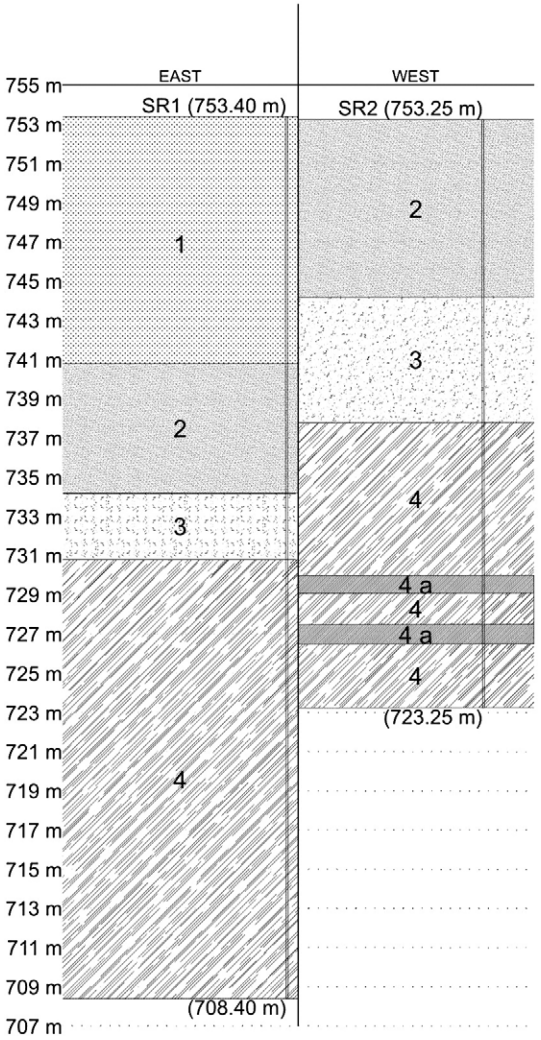

Fig. 14. Core logs of boreholes S-1 and S-2 placed on different sides of the fault F1 in Fig. 11, which suggests a fault throw of about 7 m. 1. Dense conglomerate. 2. Very dense conglomerate. 3. Moderately dense conglomerate. 4. Very dense, gravely and sandy conglomerate. 4a. Clay layer (see Section 5.1 for lithological details).

Table 2
Average properties for the different layers of Alhambra conglomerate

Layer no.	k (m/s)	Classification tests				Strength tests			From plate loading test		Pressuremeter tests			Geophysical		
		<0.08 mm (%)	w_L	I_P	USCS	σ_{ci} (kPa)	Drained direct shear test		Loading	Unloading	E_M (MPa)	p_l^* (kPa)	Φ' est. (°)	V_p (m/s)	V_s (m/s)	E_d (MPa)
							c' (kPa)	Φ'	E_m (MPa)							
1	3×10^{-7}	12.6	22	6	GC-GM				397	1772	60	2700	38	1500	800	3700
2	9×10^{-6}	22.0	24	6	GC-GM				601	2683			40	2000	960	5600
3	2×10^{-7} to f.d	27.8	22	2	SM				397	1772	33	2300	37	1500	800	3700
4	6×10^{-10} to f.d.	35.2	21	7	SC-SM GM				891	3976	115	7400	44	2400	1150	8300
4a	7.7×10^{-7}	79.4	28	11	CL	394	34.5	33.4°	109	485	42	4500	41	1500	800	3700

f.d. = free drainage. est. = estimated value. p_l* = net pressuremeter limit pressure. E_M = pressuremeter modulus. V_p = longitudinal wave velocity. V_s = transverse wave velocity. E_d = dynamic modulus. σ_{ci} = uniaxial compressive strength.

4. Very dense, gravelly and sandy conglomerate, of brown to pale gray silty fine matrix and variable permeability.
4a. One meter thick clay layers, interspersed in layer 4. Core recovery of 100%.

Talus appears at the foot of the slope (layer 5), composed of quartzose and phyllitic blocks, gravel and sand, with predominance of the sand fraction.

In Fig. 14 boreholes S1 and S2, placed at opposite sides of the fault, have been drawn. A vertical throw around 7 m is easily appreciated.

Table 2 presents a summary of the most important tests carried out on the different layers.

5.2. Conglomerate shear strength

Despite a thorough bibliographical search, only one case has been found in which the resistance of a conglomerate has been measured in an in situ direct shear test (Jiménez Salas and Uriel, 1964). The angle of internal friction measured in this conglomerate was 62°, with no cohesion. Valid estimates of the strength of conglomerates have not been found either.

Plate-loading tests have been carried out on this conglomerate (Cuéllar, 1998) pushing two plates against the opposite sides of a test pit. The test was performed at a 1m depth, where the velocity of the shear waves was 222 m/s and the dynamic modulus was 281 MPa. To find the moduli of the different cliff layers, it has been assumed that the static modulus is proportional to the dynamic modulus. The moduli obtained in Table 1 are smaller than the moduli in the tests reported by Jiménez Salas and Uriel (1964), which ranged from 8,300 to 19,000 MPa; this indicates that the conglomerate tested by these authors is harder than the Alhambra conglomerate.

Le Centre d'Études Ménard (1970) recommends a relationship between the pressuremeter limit pressure and the angle of internal friction (Φ'), out of which the following equation is deduced:

$$\phi' = 13.288 \log p_l^* - 7.86 \quad (3)$$

where p_l^* is the pressuremeter *net limit pressure* in kPa.

Using this equation and the pressuremeter limit pressure values from Table 2, the values of Φ' that appear in Table 3 are obtained.

Although Baguelin et al. (1978) quote this relationship, they point out that *at present there are no theoretical procedures to turn the pressuremeter parameters into the effective soil parameters c′ and Φ′*. Nevertheless, Baguelin et al. obtained rather good agreement (somewhat on the safe side) comparing Ménard's estimates with the results of triaxial and direct shear tests.

In San Pedro Cliff, it has only been possible to conduct uniaxial compressive strength and drained direct shear tests in the clay layer 4a (Table 2). In the drained shear test, the sample is saturated in its cell, whereas at the site the ground is only superficially saturated at times of intense rain.

The uniaxial compressive strength is related with Mohr–Coulomb parameters by the well-known equation:

$$c = \frac{q_u}{2}\frac{1 - \sin \Phi}{\cos \Phi}. \quad (4)$$

Accepting the uniaxial compressive strength of the clay layer as a minimum for the conglomerate, Table 3 shows the minimum cohesion obtained in the different layers, applying Eq. (4) to the angles of internal friction obtained from the pressuremeter limit pressure in Table 2 (hypothesis 1). In a second hypothesis, it has been assumed that the angle of internal friction was 50°, in accordance with Eq. (2): the cohesion value obtained from Eq. (4) is included in Table 3.

Table 3
Design parameters for the different layers of the Alhambra conglomerate

Layer no.	Hypothesis 1: angle of internal friction from correlations with pressuremeter limit pressure		Hypothesis 2: angle of internal friction from fault dip angle	
	Φ	c (kPa)	Φ	c (kPa)
1	38°	96	50	72
2	40°	92	50	72
3	37°	98	50	72
4	44°	84	50	72
5	(38°)	(15)	50	72

(38°) = estimated value.

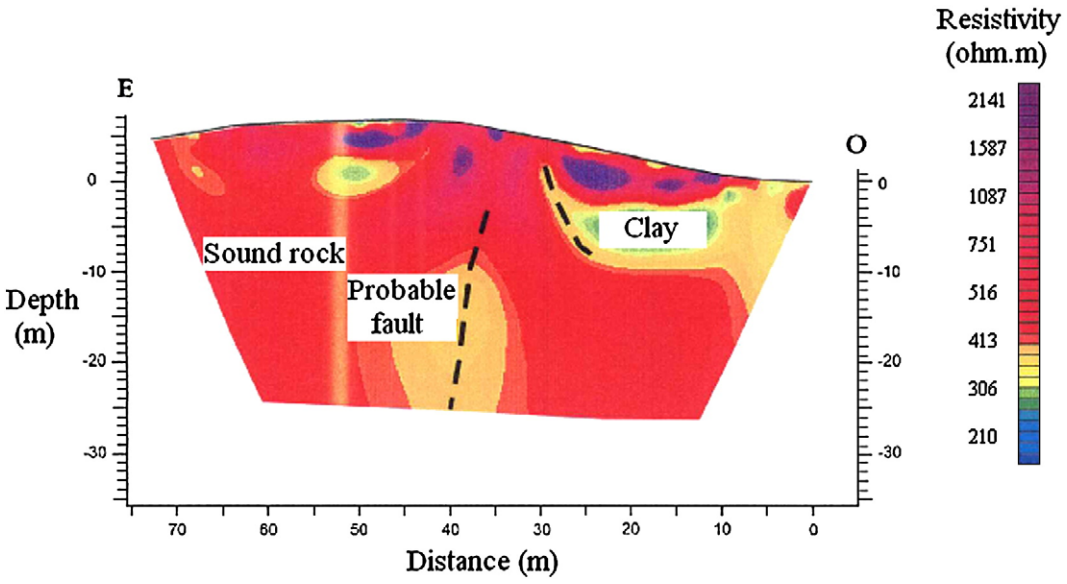

Fig. 15. Resistivity profile Te-1.

5.3. Electrical tomography

An electra 1000 transmitter was used to obtain a 72 m long resistivity profile between the two boreholes and across the suspected fault (Fig. 13) using the dipole–dipole measurement system (Sasaki, 1992).

Fig. 15 shows the resistivity profile TE-1 obtained. The factor that exerts the greatest influence on resistivity is the water content that is strongly related to ground lithology. Saturated clayey materials are characterized by low resistivity values but, when the degree of saturation is low, the resistivities are higher and may be in the range of 100 to 500 Ω m. On the other hand, while consolidated rocks with a low clay content, such as sandstones and limestones, present resistivities from several hundred up to several thousand Ω m, depending upon soundness and water content, porous conglomerates may be in the range of 200 to 1500 Ω m, and it is not an easy matter to differentiate them from dry clay. For this reason, this profile, obtained by an independent enterprise, detects the clay layer that appears in borehole S-2 (19 m apart), but not exactly at the same depth and with the same thickness. Furthermore, it must be noted that the site is in a shattered fault zone.

Taking into account the lithological homogeneity of the rocky massif, and the sub-horizontal layout of the conglomerate levels, the sub-vertical resistivity anomaly has been interpreted as a fault zone.

6. Geotechnical stabilization of the San Pedro escarpment

6.1. Previous solutions

The danger to the Alhambra wall posed by further slab failures on the cliff was foreseen long ago and, from 1520, the following solutions have been proposed and in some cases executed:

a) Embankments or walls at the foot of the cliff to protect the cliff against erosion by the river.

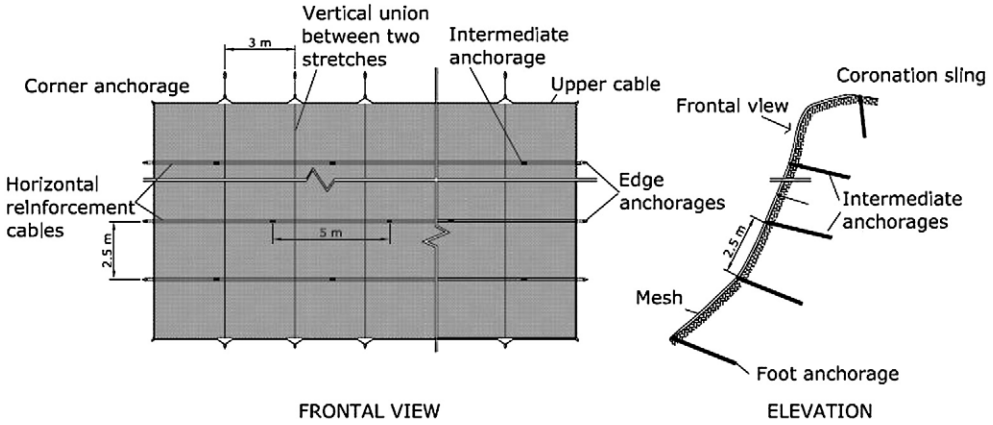

Fig. 16. Layout of high-yield stress post-tensioned wire mesh. The elevation is only a sketch. The true anchorage depths are indicated in Fig. 17.

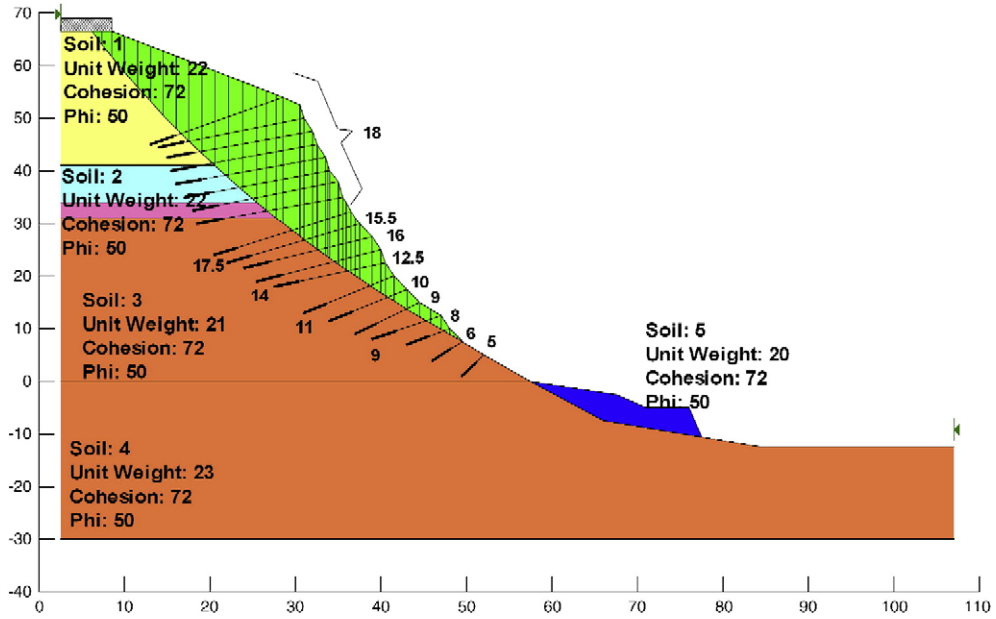

Fig. 17. Critical slip surface under dynamic conditions using Morgenstern and Price method and parameters' hypothesis 2. Anchor depth is indicated above each anchor.

b) Prohibit irrigation of the *Alhambra* forest.
c) Diversion of the river.
d) An ecological wall that will cover the dihedral, combined with Californian drains, slope sewing, reinforcement micro-piles and acrylic treatment of the slope surface to prevent erosion.
e) Grouting through a series of steel tubes sub-parallel to the slope, coupled with river regulation.

6.2. Review of proposed solutions

A desirable solution should have minimum environmental impact, with little intervention and low cost, but it should be effective.

a) It is neither necessary nor convenient to construct new embankments (in excess of the scree lying at the foot), because the problem of the floods is not so important now and in any case should be solved by regulation of the river upstream. A wall might be needed to protect the Santa Ana irrigation structure, but not the cliff.
b) If the Alhambra forest were not irrigated, its vegetation would wither.
c) A *Darro River* diversion would be unacceptable as the river is an important component of the urban landscape in a spot as beautiful as the *Carrera del Darro* street.
d) Reinforced earth or ecological walls would drastically change the present scenery. The Californian drains would need pipes to collect the drainage, whose impact would not be negligible. Acrylic treatment would necessitate removal of the loose portions and the result would not be attractive.
e) Grouting of the conglomerate is not a guaranteed solution, as the median coefficient of permeability is 2×10^{-7} m/s. Rather, it could induce new slab falls from the slope.

6.3. Adopted solution

The solution adopted by Pisa City Council intends that the tower will not lean any further, and does not try to straighten it. In the same way, remedial measures in San Pedro Cliff should consider that it is a unique geological singularity that should be preserved, but should avoid further retreat that eventually will endanger a monument, which is a World Heritage site. Solution d) however considers that San Pedro Cliff is an anomaly that needs to be corrected.

Environmental impact should be kept at a minimum. With this aim, the solution adopted has been a high-yield-stress wire mesh (Fig. 16). It is a rhomboidal mesh, with yield stress around 2000 MPa and 3 mm wire thickness, lying directly on the slope with 65 mm openings. The pressure on the slope (10 to 30 kPa) is applied by post-tensioned anchorages (Figs. 16, 17 and 19) isolated or reinforced by cables. The anchorages were GEWI bars, 40 mm thick, and their depths are indicated above each tie-rod. It would be desirable to place deeper anchorages in some

Table 4
Safety factors in static and dynamic slope calculations

Pressure on slope (kPa)	Factor of safety					
	Static			Dynamic		
	Hypothesis 1	Hypothesis 2		Hypothesis 1	Hypothesis 2	
	Morgenstern & Price	Morgenstern & Price	FE	Morgenstern & Price	Morgenstern & Price	FE
0	1.35	1.42	1.34	0.97	0.97	Fails with a=0.19 g
10	1.41	1.50		1.05	1.03	
20	1.48	1.61	1.63	1.12	1.09	1.12
30	1.55	1.70	1.64	1.17	1.16	1.13

FE = finite elements. *a* = acceleration.

places, but there are technical difficulties to do so. Double anchored cables 20 mm thick surround the treated zone.

The 65 mm mesh openings are small enough to avoid erosion of the conglomerate and to provide acceptable visual impact, especially if the present vegetation is maintained (at least the trees and shrubs) and new autochthonous plants are added.

7. Stability of slopes

The crack in the tower of Fig. 12 shows how motion towards the cliff has been detected rather far away from the cliff.

Calculations of the static and pseudo-dynamic stability of the slopes have been carried out with the parameters corresponding to hypotheses 1 and 2 in Table 3. The Geo-Slope program and the Morgenstern and Price method were used in the calculations, with different mesh pressures applied on the slope. For the pseudo-dynamic calculations, the ground acceleration applied corresponds to the 1000-year return period (0.28 g), following the recommendations of the Spanish standard for monuments (NCS-94, 1994). This standard takes into account the geographical position of the site, the return period and the shear wave velocity of the ground. Only an equivalent horizontal calculation of seismic acceleration is provided by the standard. The results are included in Table 4. In most cases, the critical slip surface penetrates inside the Alhambra walls. For no pressure on the slope, the factor of safety under dynamic conditions is less than unity with both hypotheses. Fig. 17 shows the critical slip surface under dynamic conditions, for the design pressure of 20 kPa on the slope that was finally adopted.

The calculations have been repeated using a plain-strain finite element (FE) program and a Mohr–Coulomb model, for parameters hypothesis 2 (the most reliable). The well-documented slab failure of 1985 (see Fig. 1) indicates that slides usually occur on one of the dihedral sides and are not three-dimensional. Although there is clast orientation in the direction of the fault (Fig. 9), the granular nature of the conglomerate guarantees that there is no strong strength decrease in this direction, as would happen in clay, shale or slate.

The Mohr–Coulomb material model is a model of perfect, non-associated plasticity (Plaxis, 2005). Fig. 18 shows the fixed yield surface, a hexagonal cone in principal stress space, corresponding to the six equations:

$$f_{ij} = 1/2\left(\sigma'_{ic} - \sigma'_{jc}\right) - 1/2 \ \sin \ \phi' \left(\sigma'_{ic} + \sigma'_{jc}\right) \leq 0 \qquad (5)$$

where:

$$\sigma'_{ic} = \sigma'_{i} + c' \ \cot \ \phi'.$$

In addition, the six plastic potential functions for this model are:

$$g_{ij} = 1/2\left(\sigma'_{i} - \sigma'_{j}\right) - 1/2 \ \sin \ \psi' \left(\sigma'_{i} + \sigma'_{j}\right). \qquad (6)$$

In Eqs. (5) and (6) $i = 1, 2, 3 \quad j = 1, 2, 3 \quad l \neq j$.

For stress states represented by points within the yield surface, behaviour is purely elastic and all strains reversible. The two plastic model parameters appearing in the yield functions are the well-known friction angle and cohesion c. The plastic potential functions contain a third plasticity parameter, the dilatancy angle Ψ. This parameter is required to model positive plastic volumetric increments (dilatancy) as observed for dense ground. For $c > 0$, the standard Mohr–Coulomb criterion allows for tension. This behaviour can be included in a

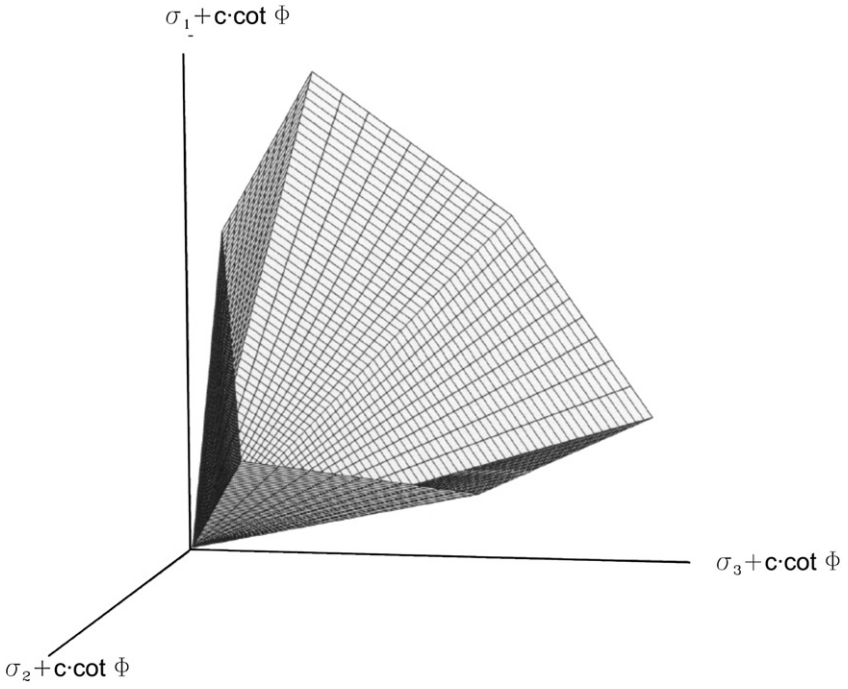

Fig. 18. The Mohr–Coulomb yield surface in principal stress space.

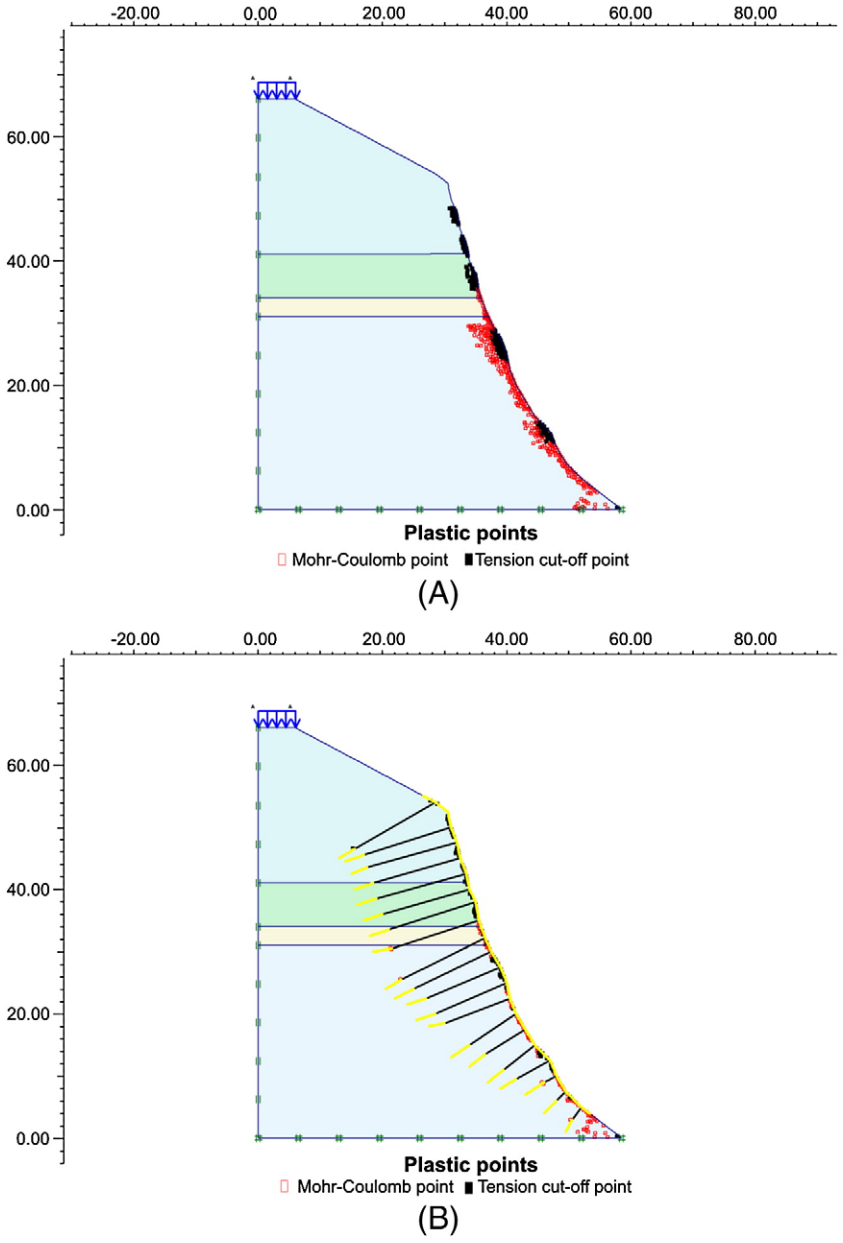

Fig. 19. Plastic and tension cut-off points. A. No mesh. B. Mesh and pre-stress.

Plaxis analysis by specifying a tension cut-off. The tension cut-off introduces three additional yield functions, defined as:

$$f_{kt} = \sigma'_k - \sigma'_t \geq 0 \tag{7}$$

with $k = 1,2,3$.

Stability calculations have been carried out with Plaxis 8.6. Plaxis computes safety factors using the *Phi-c reduction*. This method has been applied in rock mechanics by Hammah et al. (2004). Once a calculation under service loads has been performed, the ground strength parameters $\tan\Phi$ and c are successively reduced until failure of the ground structure occurs. The total multiplier ΣMsf is used to define the value of the soil strength parameters at a given stage in the analysis:

$$\sum \text{Msf} = \tan \phi_{\text{input}} / \tan \phi_{\text{reduced}} = c_{\text{input}} / c_{\text{reduced}} \tag{8}$$

with strength parameters with the subscript "input" referring to the properties entered in the material sets and parameters with the subscript "reduced" referring to the reduced values used in the analysis.

ΣMsf is set to 1.0 at the start of a calculation to set all material strengths at their unreduced values. A *Phi-c reduction* calculation is carried out using the *Load advancement number of steps* procedure. Strength parameters are successively reduced automatically until all *Additional steps* that have been set are carried out. It must be checked whether a failure mechanism has been fully developed. If that is not the case, then the calculation must be repeated with a larger number of additional steps. The best way to check this is to plot a curve on which the parameter ΣMsf is plotted against the displacement of a certain node. The maximum displacements plotted are not relevant. Usually a more or less constant value of ΣMsf is obtained, which is the safety factor value.

Safety factors obtained by this method, included in Table 4, are usually somewhat lower than the values obtained with the Morgenstern and Price calculation, because tension cut-off has been provided in the FE calculation.

Fig. 19A shows tension cut-off (points where the program has cancelled the tension stresses) and plastic points with no pre-stress. There are many plastic points near the slope. This fact explains the slab failures. Fig. 19B shows the same result with pre-stress. Plastic points are reduced and restricted to the slope line. Even more, the net prevents slab falls.

8. Environmental and aesthetical issues

From the species existing at the site, only the nettle tree (*Celtis australis*) may be considered a species of *special interest*, however, not being an element in danger of extinction. In fact, this tree is used frequently in landscaping in Granada. In addition, it is a species that colonizes on its own, on steep rocky slopes next to riverbanks.

Of the list of species that may turn up in this zone, only the common bat has the status of *significant protection*, the rest of species being out of danger. The *horseshoe snake* might also appear in the zone under study, because this is the kind of habitat it is frequent (scrubland, etc.). However, up to now it has not been detected.

The landscape environment of the restoration project is worthy of preservation, being one of the more beautiful urban strolls in the world. The walk along the right riverbank, from *Plaza Nueva* to the *Paseo de los Tristes* – known as *Carrera del Darro* – is catalogued as one of the more romantic strolls in the world. This assessment is endorsed by the international recognition held by the two hills between which the Darro River

Fig. 20. San Pedro Cliff from an immediate vision field. A. Present state. B. Computer simulation showing the Cliff after reinforcement and plant growth.

runs: Alhambra hill, where the historical monuments of the Alhambra and Generalife majestically rise, and Albaicín hill, where the popular district of the same name stands. Both have been classified as World Heritage sites by UNESCO.

For this reason, the most significant visual impact of the installation of the mesh comes from the alteration of the cultural and aesthetic value of the surroundings. The different structural elements that form the visible mesh can be coloured to blend with the cliff (ochre and brown colours), in this way favouring their integration, unlike conventional, galvanized steel meshes, which are clearly visible due to the reflection of light on the zinc coating. The elements of this mesh are thin, and it is very difficult to distinguish them at mid distance (around 100 m), as the thickness of the wires is 3 mm. Another point to consider is that, being flexible, the mesh adheres to the original profile of the slope, which is therefore unmodified. The scaffolding needed to install the mesh and the anchors, would be completely removed after installation and there would be no long-term impact.

The restoration is invisible from Alhambra hill, and only can be seen from the opposite hills of Albaicín and Sacromonte. The view from these areas has been studied: 4 vision fields have been defined according to the distance of a possible observer from the site.

The nearest field of vision is for observers located at less than 100 m: *Carrera del Darro* and *Paseo de los Tristes*. Fig. 20A shows the present state of San Pedro Cliff from an immediate vision field and Fig. 20B shows how the scene might look after reinforcement and vegetation growth. The mesh is not visible, as the thickness of the wires is only 3 mm; it is very difficult to make out the cables and the anchor heads may be seen as far-away points. The images supplied by the visualization of the project reveal that once the works are finished and the vegetation has grown, the impact of the project in relation to the aesthetic and cultural values at San Pedro Cliff should be only moderate. It will be recommended that after the maintenance period of the project has ended, pre-stressing should be checked and, if needed, replaced. In any case this proposal does not limit future possibilities.

9. Discussion and conclusions

The Alhambra (dating from the 14th C. AD) is built on the Alhambra Formation, a conglomerate, with a visible thickness of 200 m. San Pedro Cliff, located in the northern hill slope of the Alhambra forest, was formed by a combination of scour on the convex side of a river meander, loosening produced by the extensional tectonic regime, erosion, seepage coming from the *Alhambra* palace and earthquakes. At present, the base of the escarpment is covered by a debris cone that protects it from possible undercutting during flooding. The retreat of the escarpment is relatively slow, occurring at an average rate of 8 cm/year by means of soil creep and slope wash, except in the western part of the escarpment where tension joints parallel to the slope cause successive superficial slab falls.

The western part of the San Pedro escarpment corresponds to an erosional feature that utilises the anisotropy of the fault line; the fault-plane outcrops in the innermost part of the escarpment, showing a normal-fault displacement of about 7 m and NW–SE strike with NE steep dip. This fault is the most important one of a set that outcrops along the northern hill slope of the Alhambra. In some cases, the activity of these faults seems to be very recent and may be related to earthquakes. The seismic risk associated with these faults (and maybe some non-outcropping ones) appears to be moderate, as some historical damage to the Alhambra walls and the Arab barrier is reported. The most important earthquake affecting the Alhambra and neighbouring areas occurred in 1431, being responsible for the partial collapse of the Arab barrier. Moreover, the Christian barrier, built in 1526, has numerous cracks geometrically related to fault-planes outcropping in the Alhambra Formation, i.e. faults and cracks are continuous and have similar strike and dip. We hypothesize that these cracks are due to post-1526 small displacements along the faults, occurring during recent earthquakes in the region or to tectonic lateral dilation, as the barrier is so light that loads applied to the rock are negligible. In the same way, numerous cracks and collapses in the Alhambra walls appear mostly concentrated and aligned in a NW–SE strike with Christian wall cracks and faults. Nevertheless, these faults constitute mechanical discontinuities, which is a supplementary risk, because they reduce the stability of the entire massif. Moreover, the fault zones are preferential pathways for water circulation, and they suffer an increment of water erosion as compared to neighbouring areas.

Stability calculations suggest that the factor of safety under the 1000-year return period earthquake could drop below 1, and the critical slip surface could penetrate inside the Alhambra walls. So as to raise the factor of safety to values ≥ 1 (Eurocode 1, 1991), to counteract the tension and to restrain erosion, an environmentally acceptable solution is proposed, consisting of a high-yield stress wire mesh, post-tensioned by deep anchors. Simulations of the mesh suggest that the visual impact should be acceptable.

Acknowledgements

The present study has been co-financed by the *Patronato de la Alhambra y el Generalife, Confederación Hidrográfica del Guadalquivir*, and grants BIA2004-01302 and CGL2004-03333/BTE from the Research and Development Department of the MEC, partially financed by FEDER funds of the EU. The help received from Ma. Teresa Pérez and Manuel Vázquez is acknowledged.

References

Aki, M., 1965. Maximum likelihood estimate of b in the formula $\log N = a - bM$ and its confidence limits. Bull. Earthq. Res. Inst. Univ. Tokyo 43, 237–239.

Ayala-Carcedo, F.J., Rodríguez-Ortiz, J.M., Prieto Alcolea, C., Durán Valsero, J.J., Lamas Romero, J.L., Rubio-Amo, J., 1986. Mapa previsor de riesgos por inundaciones en núcleos urbanos de Andalucía y Extremadura. IGME, Madrid.

Azañón, J.M., Azor, A., Booth-Rea, G., Torcal, F., 2004. Small-scale faulting, topographic steps and seismic ruptures in the Alhambra (Granada, southeast Spain). J. Quart. Sci. 19, 219–227.

Baguelin, F., Jézéquel, D.H., Shields, D.H., 1978. "The Pressuremeter and Foundation Engineering". Trans. Tech. Publications, Aedermansdorf, Switzerland.

Bender, B., 1984. Incorporating acceleration variability into seismic hazard analysis. Bull. Seism. Soc. Am. 74, 1451–1462.

Castillo, A., 2007. CSIC, Granada. Private communication.
Cedex, 1993. Caracterización geotécnica de las condiciones de cimentación del conjunto monumental de La Alhambra y Generalife. Report No. 3. Centro de Estudios y Experimentación de Obras Públicas, Laboratorio de Geotecnia, Madrid.
Centre d'Etudes Ménard, 1970. Détermination de la Poussée Exercée par un Sol sur une Paroi de Soutènement. Publication D/60/75.
Cuellar, V., 1998. Caracterización dinámica de los materiales. Cuad. Alhambra 33–34, 105–114.
Eurocode 1, ENV, 1991. Actions on Structures. British Standards. -1.
Ferrill, D.A., Morris, A.P., 2003. Dilational normal faults. Eng. Geol. 25, 183–196.
Galindo-Zaldívar, J., Jabaloy, A., Serrano, I., Morales, J., González-Lodeiro, F., Torcal, F., 1999. Recent and present-day stresses in the Granada Basin (Betic Cordilleras): example of a late Miocene — present-day extensional basin in a convergent plate boundary. Tectonics 18, 686–702.
Galindo-Zaldívar, J., Gil, A.J., Borque, M.J., González-Lodeiro, F., Jabaloy, A., Marín-Lechado, C., Ruano, P., Sanz de Galdeano, C., 2003. Active faulting in the internal zones of the central Betic Cordilleras (SE, Spain). J. Geodyn. 36, 239–250.
Galbis, J., 1932. Catálogo sísmico de la zona comprendida entre los meridianos 5° E y 20° W de Greenwich y los paralelos 45° y 25°. Madrid, Dirección General del Instituto Geográfico Catastral y de Estadística.
Hammah, R.E., Curran, J.H., Yacoub, T., Corkum, B., 2004. Stability analysis of rock slopes using the finite element method. EUROCK 2004 & 53 Geomechanics Colloquium, Schubert.
Jiménez Salas, J.A., Uriel, S., 1964. Some recent Rock Mechanics testing in Spain. 8th Cong. Large Dams, Edinburgh, vol. 1, pp. 995–1021.
Justo, J.L., Vázquez, N., Durand, P., 2005. Proyecto de restauración del Tajo de San Pedro de La Alhambra de Granada". Confederación Hidrográfica del Guadalquivir y Patronato de La Alhambra y Generalife, Seville, Spain.
Lombardi, A.M., 2003. The maximum likelihood estimator of *b*-value for mainshocks. Bull. Seismol. Soc. Am. 93 (5), 2082–2088.
López-Casado, C., Peláez-Montilla, J., Henares-Romero, J., 2001. In: Sanz de Galdeando, J.C., Peláez Montilla, J.A., y López Garrido, A.C. (Eds.), Sismicidad en la cuenca de Granada. In "La Cuenca de Granada: estructura, tectónica activa, sismicidad, geomorfología y dataciones existentes". CSIC-Univ., Granada, pp. 148–157.
Martín, A.J., 1984. Riesgo Sísmico en la Península Ibérica. Ph.D. Thesis, University (Complutense) of Madrid.
Martínez, J.M., 1998. Instrumentación y análisis de resultados. Cuad. Alhambra 33–34, 79–103 Granada.
Morales, J., Singk, S.K., Ordaz, M., 1996. Analysis of the Granada (Spain) earthquake of 24 June, 1984 ($M=5$) with emphasis on seismic hazard in the Granada Basin. Tectonophysics 257 (2–4), 253–263.
Morales, J., Serrano, I., Jabaloy, A., Galindo-Zaldívar, J., Zhao, D., Torcal, F., Vidal, F., González-Lodeiro, F., 1999. Active continental subduction beneath the Betic Cordillera and the Alboran Sea. Geology 27, 735–738.
Muñoz, D., Cisternas, A., Udías, A., Mezcua, J., Sanz de Galdeano, C., Morales, J., Sánchez-Venero, M., Haessler, H., Ibáñez, J., Buforn, E., Pascual, G., Rivera, L., 2002. Microseismicity and tectonics in the Granada Basin (Spain). Tectonophysics 356, 233–252.
Page, R., 1968. Aftershocks and microaftershocks of the great Alaska earthquake of 1964. Bull. Seismol. Soc. Am. 58, 1131–1168.
Plaxis, 2005. In: Brinkgreve, R.B.J., Broere, W. (Eds.), Plaxis 3-D Foundation. Version 1.5 manual. Delft Univ. and Plaxis BV, The Netherlands.
Rodríguez-Fernández, J., Sanz de Galdeano, C., 2006. Late orogenic intramontane basin development: the Granada basin, Betics (southern Spain). Basin Res. 18, 85–102.
Rodríguez-Fernández, J., Sanz de Galdeano, C., Fernández, J., 1989. Genesis and evolution of the Granada Basin (Betic Cordillera, Spain). In: Thauasuthipitak, TP, Ounchanum, P (Eds.), Intermontane basins. Geology and resources, pp. 294–305.
Sanz de Galdeano, C.J., Peláez Montilla, A., López Casado, C., 2003. Seismic potential of the Main Active Faults in the Granada Basin (Southern Spain). Pure Appl. Geophys. 160 (8), 1537–1556.
Sasaki, Y., 1992. Resolution of resistivity tomography inferred from numerical simulation. Geophys. Prospect. 40 (4), 453–463.
Tercedor, M., 1951. La tectónica de la depresión granadina en relación con su elevada sismicidad. Estud. Geol. 7, 29–70.
Torcal, F., Posadas, A.M., Serrano, I., 1999. Simulating a seismic series using geostatistical and stochastic methods: application to the seismic series in the Alboran Sea (1997 June 24). Geophys. J. Int. 139, 726–742.
Utsu, T., 1965. A method for determining the value of *b* in the formula log $N=a-bM$ showing the magnitude–frequency relation for earthquakes (with English summary). Geophys. Bull. Hokkaido Univ. 13, 99–103.